# A model for the ablation rate of a solid hydrogen pellet in a plasma

NUCLEAR FUSION 17 3 (1977)

# A MODEL FOR THE ABLATION RATE OF A SOLID HYDROGEN PELLET IN A PLASMA

P.B. PARKS*, R.J. TURNBULL, C.A. FOSTER+
Department of Electrical Engineering,
University of Illinois at Urbana-Champaign,
Urbana, Illinois,
United States of America

ABSTRACT. It is shown that the ablation of a solid hydrogen pellet subject to a plasma is likely to produce a quasi-steady dense neutral gas cloud. The total integrated density of the cloud is such that the plasma electrons lose essentially all their energy in the cloud. The electron energy flux is degraded by inelastic collisions and elastic backscattering with the neutral molecules, providing local heating and acceleration of the neutral gas. Only a small fraction of the energy flux reaches the surface of the pellet, raising the pellet's surface temperature to a point where the energy flux at the pellet's surface is in balance with the energy lost through vaporization. The vaporization rate, in turn, determines the total integrated neutral gas cloud density. The scaling laws derived from the model indicate that the pellet lifetime varies as: $\tau_p \sim T_e^{-1.71} n_e^{-1/3} r_{p0}^{5/3}$, where $\tau_p$ is the lifetime of the pellet and $T_e$, $n_e$, and $r_{p0}$ are the electron temperature, density of the plasma, and initial pellet radius, respectively. A good agreement is found between this model and the ORMAK pellet injection experiment.

## 1. INTRODUCTION

The possibility of using small frozen deuterium-tritium pellets to refuel fusion reactors was first conceived by Spitzer and Tonks [1] in the early days of fusion research. Their main idea was that the preservation of the self-shielding by the ablation cloud ions and electrons against free spherical dispersal by means of self-consistent fields created by motion of the ionized cloud across the magnetic field would increase the pellet lifetime. Later Rose [2] introduced the idea that a high-$\beta$ magnetic bubble caused by the pressure of the charged particles in the ablation cloud would be formed around the pellet, thereby diverting the incoming electron flux around the pellet, enhancing its lifetime. In contrast to Rose's balloon model, Chang [3], using a "magnetic nozzle" model, concluded that the shielding becomes more effective when the $\beta$ of the ablation cloud is low. Recently, Gralnick [4,5] postulated that an ionizing vaporization front is driven into the pellet by the hot incident reactor electrons and the resulting cold ablation plasma absorbs energy from the electrons, thereby reducing the ablation rate of the pellet.

Generally speaking, the above models have all assumed a high degree of ionization of the ablation cloud surrounding the pellet. If we consider present-day and proposed tokamaks, it appears that the amount of ionization will be negligible within a few pellet radii of the pellets' surface. Since this is where the shielding is most pronounced, a neutral ablation model should be used to calculate the pellet lifetimes.

The model we propose is that the molecules are ablated off the pellet as neutrals. The resulting neutral cloud then undergoes an expansion away from the pellet. The incoming plasma electrons are slowed down by the neutral cloud, reducing the energy flux to the pellet and thus increasing its lifetime. Quasi-steady-state conditions are assumed. It will be shown later that all problems of fusion interest allow the quasi-steady-state assumptions.

The plasma electron energy provides a thermal energy source to the ablation cloud. Some of this energy goes into the kinetic energy of the ablation cloud with the remainder going into increasing the temperature of the cloud. The cloud molecules are thus continuously accelerated as they move away from the pellet surface. The dynamics are illustrated in Fig. 1a.

* Present address: General Atomic Company, San Diego, California 92138, USA.
+ Present address: Oak Ridge National Laboratory, Oak Ridge, Tennessee 37830, USA.

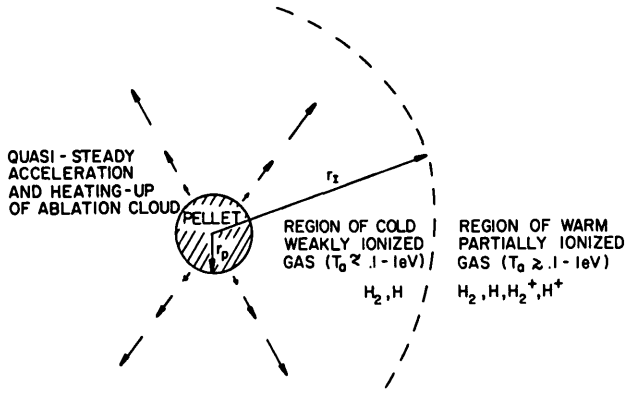


*FIG.1a. Interaction of pellet with plasma. The pellet's ablation cloud is continuously ionized by electron impact. Dissociative recombination occurring in the cold dense portion suppresses the degree of ionization. The ionization radius, $r_I$, would be the surface in the cloud where the fraction of neutrals is $\sim 1/e$ if recombination is neglected.*

In Section 2 we deal with some overall considerations related to the problem. In Section 3 a self-consistent solution to the ablation rate is obtained by deriving a simple energy transport equation for electrons slowing down and scattering in molecular hydrogen of arbitrary density. The results of this section are then applied in Section 4, where the dynamics of the phase transition are developed. In Section 5 an approximate solution is found for the heating and expansion of the ablation cloud.

Scaling laws are presented in Section 7 which relate the ablation rate and the lifetime to the initial pellet radius and plasma electron temperature and density. A comparison with the existing experimental evidence for the lifetime of a pellet injected into a plasma is made and good agreement between theory and experiment is found.

## 2. GENERAL CONSIDERATIONS

When a pellet is subject to plasma, it is bombarded by electrons, ions, and radiation. If the electron and ion temperatures are equal, the electron energy flux is the dominant form of energy transport to the pellet since the ratio of the electron-to-ion energy flux is $\sqrt{m_i/m_e}$ (where $m_i$ and $m_e$ are the masses of the ions and electrons, respectively). It can indeed be shown that the ions are found to be even less effective than the electrons since their ranges are shorter by a factor of $\sim m_e/m_i$. The pellet and its surrounding ablation cloud are transparent to the hard thermal radiation in the plasma. In addition, this radiation is several orders of magnitude less than the electron energy flux [2]. Therefore, the plasma electrons are the primary energy carriers to the pellet.

With the above in mind, the pellet ablation process may be described as follows: electrons strike the surface of the pellet, causing vaporization. The freshly formed vapour – hereafter referred to as the "ablation cloud" – consisting of neutral molecules flows away from the surface of the pellet in a more or less spherical manner. The density of the ablation cloud, $\rho(r)$, falls by *at least* $r^{-2}$ for a spherical expansion. Because of the rapid decrease in density of the vapour for a spherical expansion and the fact that the vapour flow velocity is significantly greater than the pellet surface recession speed, a situation arises such that the establishment of the neutral vapour cloud occurs in a time scale which is almost negligible compared to the time for the pellet's radius to change appreciably. The pellet will therefore vaporize at a rate determined by its *instantaneous* radius and the instantaneous external energy flux. This consideration admits the use of a "quasi-steady" approximation.

In all subsequent analyses, the pellet's motion through the plasma will be neglected for two reasons. First, the mean free path of the electrons in the plasma is much larger than the pellet's radius. Further, the velocity of the pellet is highly subsonic with respect to the plasma ions and electrons. Therefore a shock layer which would divert plasma from the surface of the pellet does not develop ahead of the pellet. This consideration sets the present problem apart from typical problems in atmospheric re-entry. The pellet's motion plays a part only insofar as the plasma parameters such as temperature and density vary along the pellet trajectory.

Fortunately, for a wide class of plasma conditions the gradients in the energy flux as seen by the pellet as it moves through a non-uniform plasma are weak enough to satisfy the quasi-steady approximation for the pellet ablation process. A semi-empirical qualification for the above statement to be valid is given by:

$$\left| \frac{d\ln q_o}{dx} \frac{V_p}{\overline{v(r)}} r_p \right| \ll 1 \qquad (1)$$

where $d\ln q_0/dx$ is the logarithmic change in the external (unattenuated) electron energy flux, $q_0$, along the pellet's trajectory, $V_p$ is the velocity of the pellet, and $\overline{v(r)}$ is the average flow velocity of the ablation cloud.

If $V_p$ is of order $10^4-10^6$ cm/s and $\overline{v(r)} \cong 10^5$ cm/s, then Eq.(1) is easily satisfied. Therefore a quasi-steady-state model will be used throughout the remainder of this paper.

The incident electrons interacting with the neutral ablation cloud partition their energy into basically four processes [6]: the loss to primary ionization threshold from which secondary electrons result; the energy of the secondary electrons; dissociative ionization from which only low energy atoms emerge unable to produce more ions; and finally, discrete-state excitations. Reference [6] gives the partition of the incident electron energy into these various processes.

The cross-sections for direct ionization of $H_2$ into e - $H_2^+$ pairs is over an order of magnitude larger than the dissociative ionization, in which case $H^+$ results [7].

The $H_2^+$ ions can undergo several subsequent reactions. The most efficient reaction is dissociative recombinations with thermalized secondary electrons in the ablation cloud. Energetic H atoms arise which thermalize rapidly in the ablation cloud. As shown in Section 7, Eq.(41) the ablation cloud has a temperature of about 1 eV for fusion plasma conditions. For electrons of 1 eV the dissociative recombination cross-section is quite large $\sim 6.4 \times 10^{-16}$ cm [8, 9]. The product $\langle\sigma v\rangle_{\text{recombination}}$ is about an order of magnitude higher than $\langle\sigma v\rangle_{\text{ionization}}$ by incident electron impact. Clearly the density of thermalized primary electrons and secondary electrons is much higher than the incident electrons density in the ablation cloud. Thus recombination of the $H_2^+$ ion is very fast. There are two additional but less important processes competing for the $H_2^+$ ion. The first is dissociation by incident electron impact creating both H and $H^+$. The cross-section for this process is $\sim 2$ times the e - $H_2$ ionization cross-section for incident electron energies $\gtrsim 500$ eV [10]. Finally the $H_2^+$ ion can undergo an exothermic ($\sim 1.6$ eV) reaction with $H_2$ forming H and $H_3^+$ [11]. From these processes most of the energy which went into ionization eventually goes into heating of the ablation cloud.

The discrete-state excitation leads eventually to heat also. This is because collisions between the neutrals in the ablation cloud under most conditions occur in a time scale much shorter than the time for the excited molecules or atoms to re-emit by spontaneous emission. Therefore, the excitation energy is distributed among the ablation species as an additional kinetic energy of the molecules.

Therefore, we expect that nearly all of the incident electron's energy (including secondary electrons) is degraded into thermal energy of the ablation cloud. It is this heating which drives the flow outward. At some point in the flow the molecules have reached a distance at which point most of them have become ionized by electron impact as described above. We call this distance the "ionization radius". An estimate of the ionization radius, denoted by $r_I$, can be obtained as follows. Let v(r) be the gas-dynamic flow velocity of the ablation cloud at a radial distance r from the centre of the pellet. Without treating recombination, $r_I$ can be estimated according to:

$$\int_{r_p}^{r_I} \frac{dr}{v(r)} = \tau_{ei} \tag{2}$$

where $r_p$ is the pellet radius, and $\tau_{ei}$ is the lifetime of a neutral molecule against electron ionization. As shown in Section 7, Table I, $r_I/r_p$ is quite large even for plasmas characteristic of present-day or near-term tokamak reactors [12].

From the above, if $r_I/r_p \gg 1$, justification is given to the mechanism of continuous absorption of the electron energy flux in the predominantly neutral portion of the ablation cloud near the surface.

Since, as will be shown in Section 7, a large fraction of the incident electron energy flux is absorbed in the ablation cloud, the average incident electron energy has been degraded enough so that by the time the electron strikes the pellet surface, it has an effective range in the solid of the order of a micrometre or less even for energetic plasmas. Heat is developed in a thin layer underneath the surface and is conducted back to the surface and simultaneously into the interior of the pellet. The part conducted back to the surface sustains the vaporization. The velocity of heat transport into the interior of the pellet after a time t is of the order $(\alpha/t)^{1/2}$ where $\alpha = 0.003$ cm$^2$/s is the thermal diffusivity for liquid hydrogen [13]. (The term $\alpha$ for the liquid instead of the solid phase is taken here because conduction in the solid could only raise the interior temperature up to the triple point.) For example, for a pellet of radius 300 $\mu$m subjected to a plasma with $T_{e0} = 2000$ eV and $n_{e0} = 4 \times 10^{13}$ cm$^{-3}$ the lifetime is 26 $\mu$s and the surface regression speed is $\cong 10^3$ cm/s. Taking $t \sim 26$ $\mu$s, $(\alpha/t)^{1/2} = 10$ cm/s. It is concluded that the heat conduction does not permit an adequate outlet of heat into the pellet interior. Thus, it is insignificant in the energy balance at the surface, other than maintaining a relatively thin layer of heated solid or liquid near the surface at a temperature which is determined by the evaporation rate.

Concomitant to the vaporization and neutral vapour-shielding is the possible charging of the pellet and its dense ablation cloud resulting in an electrostatic shielding effect as first suggested by Spitzer [1]. In Spitzer's model the negative equilibrium potential on the pellet is such that the incident electron and ion currents to the pellet just balance. Grâlnick [4] showed however, that the ions should be stopped by the pellet's ablation cloud, whereas the electrons of course penetrate. The model presented here is in agreement with this claim.

In the light of this, we feel that the incident electron current must be balanced by the "returning" scattered and degraded electrons which are almost entirely deposited throughout the neutral ablation cloud. These returning electrons set up electric fields in the ablation cloud. The numerous short-range secondary electrons which are created by primary electron impact and undergo subsequent thermalization will attempt to suppress these electric fields to the extent of their mobility in the dense ablation cloud. (The ions are relatively immobile in the frame of the flow.) This suppression of the field can be countered by the rapid dissociative recombination processes so as to drain off these secondaries. The net effect of the above events could lead to a negatively charged ablation cloud.

The negative charging of the pellet is possible also. Recently Sorensen [14] has found that without a surface charge the secondary electron emission coefficient for solid deuterium $\epsilon < 1$ for incident electron energies above $\sim$ 500 eV. The charging aspect of the pellet ablation problem deserves further study. Pellet charging is neglected in this paper.

Because of the extremely low degree of ionization in the ablation cloud near the pellet, the influence of the magnetic field on the expansion of the ablation cloud is also not considered in this study. Its presence does, however, direct the electrons as they slow down and scatter in the cloud, and concurrently introduces an anisotropy to the heating of the ablation cloud. This anisotropy will at least be partially accounted for in this study.

## 3. TRANSPORT OF PLASMA ELECTRONS THROUGH THE NEUTRAL ABLATION CLOUD

Many authors have studied the transport of electrons through matter [15–17]. For our purposes, an analytic transport model of the electron energy flux at any given point in the ablation cloud is needed. The model will be coupled with the gas-dynamic motion of the ablation cloud. The model should include the physical effects of large angle backscatter and cumulative small angle scatterings of electrons on hydrogen as well as slowing down in a non-uniform background density.

Plasma electrons encountering the pellet's ablation cloud lose energy through inelastic processes such as ionization and excitation of the neutral hydrogen molecules and simultaneously undergo elastic scattering. The electrons, which are travelling along the magnetic field lines, have a spectrum of pitch angles with respect to the magnetic field. In progressing a distance along a field line threading the cloud, electrons with large pitch angles will scatter and slow down more than those with small pitch angles. In the inelastic collisions the direction of the electrons can be assumed to be unaltered because the differential scattering cross-section is so strongly peaked at small scattering angles [18], i.e. the electrons lose energy but essentially continue on with the same pitch angle. In an elastic collision the electron's pitch angle changes, but its energy does not change appreciably due to the small electron-to-molecule mass ratio.

In the following derivation for the transport of the electron energy flux, we assume that the electrons stick to the field lines. This means that a "pencil beam" of electrons, which are contained within an elemental flux tube threading the ablation cloud, remains in that flux tube. Inherent in this assumption is that the electron gyro-radius must be much less than the pellet radius so that the neutral cloud density variation transverse to the magnetic field can be neglected. For example, if the magnetic field strength is 50 kG then this assumption becomes $6.6 \times 10^{-5} \sqrt{T_{e0}}/r_p \ll 1$, where $T_{e0}$ is the electron plasma temperature in eV, and $r_p$ is the pellet radius in cm. This almost always holds for combinations of

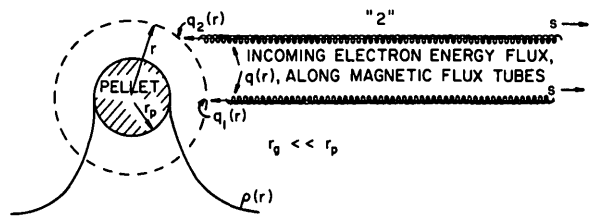


*FIG.1b. Geometry of electron energy flux deposition in ablation cloud. Provided that cloud density, $\rho(r)$, is spherically symmetric, the total integrated cloud density from $s = \infty$ up to the surface r along any two given flux tubes "1" and "2" is approximately equal. Thus $q_1(r) \cong q_2(r)$.*

plasma temperatures and pellet radii of interest. For simplicity, only those electrons which are headed towards the pellet (forward flux) are considered. Electrons which are turned around (backward flux) by elastic collisions are no longer considered, because their contribution to the total energy flux is small; the "double backscattering" process reduces their energy to essentially zero.

Let us consider the energy flux of electrons moving towards the pellet within an elemental flux tube threading the ablation cloud. From Fig.1b 's' denotes the coordinate along any given flux tube. Assuming Maxwell-Boltzman statistics apply for the plasma electrons far away from the pellet which have temperature $T_{e0}$ and density $n_{e0}$ then the unattenuated electron energy flux $q_0$, is

$$q_o = \frac{n_{eo}\bar{V}_{eo}}{4} \cdot E_o \tag{3}$$

where $v_{e0} = \sqrt{(8kT_{e0}/\pi m_e)}$ and $E_0 = 2kT_{e0}$.

As an approximation, the distribution of electrons is replaced with an equivalent mono-energetic flux of electrons with average energy $E_0$. Assuming that these mono-energetic electrons lose their energy continuously as they enter the ablation cloud, a relation between the distance an electron travels along a flux tube and its energy is given by

$$\frac{dE}{ds} = \frac{n(s)L(E)}{< \cos\theta >} \tag{4}$$

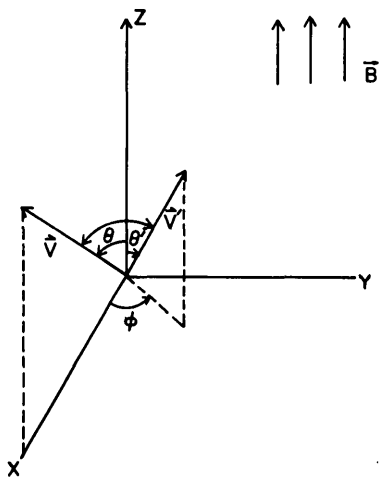


*FIG.2. Collision angles in B-field for elastic scattering. Z-axis is oriented towards pellet. $\theta(\theta')$ is pitch angle before (after) scattering at origin. $|\vec{V}| \cong |\vec{V}'|$. For backscattering $\pi > \theta' > \pi/2$.*

where n(s) is the density of neutral hydrogen molecules and L(E) is the energy-dependent loss function. The $\langle\cos\theta\rangle$ term in Eq.(4) accounts for the average pitch angle which, if weighted with an assumed isotropic distribution, is approximated by 1/2.

*Pitch angle* scattering removes electrons from the forward flux. Let $\sigma_B(\theta,E)$ be the cross-section for electrons removed (backscattered) by suffering a single elastic collision which sends an electron with initial *pitch angle* $\theta$ and energy E anywhere into the domain $(\pi/2,\pi)$ (see Fig.2). $\sigma_{MS}(E)$ is the cross-section for scattering, considering cumulative small-angle elastic collisions which lead to a total mean square deflection of $\cong 90°$. The derivations of $\sigma_B(\theta,E)$ and $\sigma_{MS}(E)$, which follow in the Appendix make use of the differential elastic scattering cross-section, $d\sigma(\xi)/d\Omega$, based on the Born approximation [18]. They are then adjusted to reflect the experimentally determined values for the total elastic scattering cross-section [19].

The forward particle flux, $\phi(s)$, of these mono-energetic electrons along a flux tube is governed by the following equation:

$$\frac{d\phi(s)}{ds} = \phi(s)n(s)\hat{\sigma}_T[E(s)] \tag{5}$$

where $\hat{\sigma}_T[E(s)]$ is the energy-dependent effective elastic scattering transport cross-section. Again, approximating the pitch angle distribution by its average value, $\hat{\sigma}_T(E)$ is defined as

$$\hat{\sigma}_T(E) = 2\,\sigma_{MS}(E) + 2\int_o^{\pi/2} \sin\theta\;\sigma_B(\theta, E)d\theta \tag{6}$$

The boundary condition on Eq.(5) is $s \to \infty$, $\phi \to (n_{e0}\bar{v}_{e0})/4$.

The differential form of the forward electron energy flux $q(s) = \phi(s)E(s)$ is simply

$$\frac{1}{q}\frac{dq}{ds} = \frac{1}{\phi}\frac{d\phi}{ds} + \frac{1}{E}\frac{dE}{ds} \tag{7}$$

Substituting Eq.(5) into Eq.(7) and making a variable change with the help of Eq.(4) we have after integration

$$q(s) = q_o \frac{E(s)}{E_o} \exp \left[ \int_{E(s)}^{E_o} 1/2\hat{\sigma}_T(E')\,L(E')^{-1}dE' \right] \tag{8}$$

where E(s) is given according to

$$1/2\int_{E(s)}^{E_o} dE'L(E')^{-1} = \int_s^\infty n(s')ds' \qquad (9)$$

Since the density of the ablation cloud is expressed in terms of the radial coordinate r we replace s by r in Eqs (4–9). This is justified since it can be easily shown geometrically that the total integrated cloud density from $s = \infty$ up to any spherical surface r along any two given flux tubes "1" and "2" is equal to within a few per cent. (Refer to Fig. 1b.)

The electron loss function, L(E), used in the above expressions, has been studied extensively for molecular hydrogen by Miles et al. [20], who obtained accurate semi-empirical cross-sections for the discrete excitation, ionization, and dissociation processes. In this way L(E) can be constructed from a knowledge of the various individual cross-sections which characterize the inelastic collisions. Miles fitted L(E) to a versatile expression which is accurate down to 20 eV, viz.,

$$L(E) = \frac{a_o z}{2R_e}\left[\left(\frac{E}{A}\right)^{\Omega} + \left(\frac{E}{B}\right)^{M} + \left(\frac{E}{C}\right)^{\Lambda}\right]^{-1} \text{ ev - cm}^2 \qquad (10)$$

where $a_0 = 6.514 \times 10^{-14}$ cm$^2$eV$^2$, $R_e$ is the Rydberg energy (13.6 eV), and z = 3.6. The constants are:

$$A = 100 \text{ eV}, \quad B = 60.0 \text{ eV}, \quad C = 48.87 \text{ eV}$$

$$\Omega = .823 \quad , \quad M = -.125 \quad , \quad \Lambda = -1.938$$

Using the results in the Appendix, $\hat{\sigma}_t(E)$ is computed from Eq. (6). The results were fitted to a convenient form, viz.,

$$\sigma_t(E) = \begin{cases} \dfrac{\sigma_1}{E^p} - \dfrac{\sigma_2}{E^r} & E \geq 100 \text{ eV} \\ \dfrac{1.1 \times 10^{-14}}{E} & E \leq 100 \text{ eV} \end{cases} \qquad (11)$$

where $\sigma_1 = 8.8 \times 10^{-13}$, $\sigma_2 = 1.62 \times 10^{-12}$, p = 1.71, r = 1.932, and E is in electron volts.

Figure 3 illustrates $E\hat{\sigma}_t(E)$ and L(E) versus energy. The comparable effects of scattering and slowing down on the total energy flux degradation are shown.

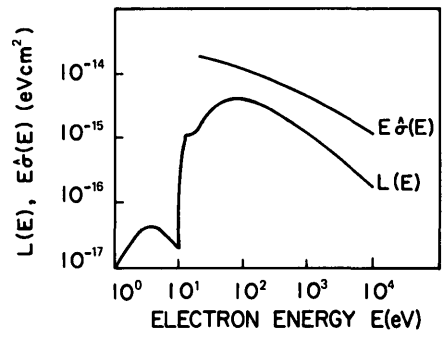


*FIG. 3. Electron loss function L(E) and effective transport cross-section for elastic backscattering $\hat{\sigma}(E)$ as function of energy E.*

## 4. SURFACE ABLATION DYNAMICS AND THE INTEGRATED CLOUD THICKNESS

Electrons which have made their way through the ablation cloud deposit their energy on the pellet's surface. The surface temperature is raised, which induces vaporization of $H_2$ molecules. Let $q_0$ be the unattenuated electron energy flux far away from the pellet ($r \to \infty$), and $q_1$ the degraded energy flux just at the pellet's surface ($r = r_p$). The fraction, $f_H$, of the energy flux, $q_1$, which goes into heat at the pellet surface giving rise to the elevated surface temperature and the phase transition can be shown to be

$$f_H = 1 - \frac{I}{W_o(E_1)} \qquad (12)$$

where $E_1$ is the average final energy of the electron which strikes the pellet surface; I, the ionization threshold for products of $H_2^+$, 15.42 eV; and $W_0(E_1)$, the incident energy $E_1$ divided by the total number of ion-electron pairs which are produced as the electrons slow down completely. For cases when $E_1$ is greater than 200 eV, $f_H = 0.576$. The mean radiative lifetime for excited $H_2$ molecules is on the order of $10^{-9}$ s [21], and the mean free path for line radiation is about 400 Å [22] in liquid or solid $H_2$. Because the average range of an electron at the pellet surface is of the order of a few micrometres the excitation radiation is absorbed. A similar argument can be applied to the secondary electrons created in the heated layer.

Equation (12) assumes that no dissociative recombination of the newly created e - $H_2^+$ pairs occurs in the liquid-heated layer on the pellet's surface. It is not clear whether one can apply the previously mentioned recombination coefficient for thermalized electrons in

a low-temperature liquid or solid (~ 20–30K). In this sense, $f_H$ as given by Eq.(12) is actually a lower limit. Since more than half of the incident energy to the pellet surface appears to go into heat and since the energy needed to vaporize a molecule is more than three orders of magnitude less than the energy needed to ionize it, we conclude that only a very small number of molecules (< 0.1 per cent) leave the surface in an ionized state. It is for this reason that we conclude that the ablation cloud is predominantly neutral near the pellet surface.

Because of the spiraling of the electrons around the magnetic field lines, the actual energy flux falling upon the pellet surface is reduced by not more than half of its value in the case with no magnetic field, depending upon the ratio of the pellet radius to the average gyro-radius of the electron with energy $E_F$ striking the pellet. A detailed analysis of this effect has been studied and for most cases of interest $f_B$, the energy flux entering the pellet, normalized to the case where no magnetic field is present and a Maxwellian distribution of electrons is assumed at the surface of the pellet, is found to be about 0.5–0.6 [23].

With the above considerations in mind, the energy balance at the pellet surface in the steady state can be shown to be given by:

$$q_1 f_H f_B = \rho_o \dot{r}_p \left[ \frac{U_s}{m_{H_2}} + \int_{T_o}^{T_s} C_p(T)\,dT \right] \qquad (13)$$

where $U_s$ is the sublimation energy, (0.01 eV/molecule), $m_{H_2}$ is the mass of a hydrogen molecule, $T_s$ is the pellet surface temperature, $T_0$ the pellet interior temperature (≅ 10–12K), $\rho_0$, the solid (or liquid) density, and $\dot{r}_p$ the rate of change in the pellet radius. $C_p(T)$ is the heat capacity at constant pressure. For solid hydrogen $C_p(T) \cong C_0 T^{3/2}$; for liquid hydrogen $C_p(T) \cong C_1 + C_2 T$ [24]. Without consideration of re-radiation from the surface Eq.(13) is similar to other standard forms regarding surface ablation; for example, the ablation of meteors in the upper atmosphere [25, 26].

The specific enthalpy content of the heated surface layer, $\int_{T_0}^{T_s} C_p(T)dT$, becomes comparable to $U_s/m_{H_2}$ when $T_s$ is above ≅ 20 K.

At the completion of bond rupture at the surface, the vapour just created is at cryogenic temperatures and has a total specific enthalpy $h_{t_1} = h_1 + V_1^2/2$, which must be equal to the specific enthalpy content of the heated surface layer. If ideal gas law behaviour is assumed, i.e. $h_1 = \gamma k T_1/(\gamma-1)m_{H_2}$, then

$$\int_{T_o}^{T_s} C_p(T)\,dT = h_{t_1} = \left[ \frac{1}{(\gamma-1)} + (\tfrac{1}{2})M_1^2 \right] \frac{\gamma k T_1}{m_{H_2}} \qquad (14)$$

Here $\gamma$ is the ratio of specific heats and $M_1$ is the Mach number for the initial vapour flow. Equation (14) provides the connection between the surface temperature, vapour temperature, and initial Mach number of the flow.

Conservation of mass at the pellet surface, assuming $\dot{r}_p \ll v_1$ is simply

$$\rho_1 v_1 \simeq \rho_o \dot{r}_p \qquad (15)$$

where $\rho_1$ is the ablation cloud density just at the surface in g/cm$^3$ and the velocity $v_1$, of the flow just at the pellet surface is:

$$v_1 = M_1 \sqrt{\frac{\gamma k T_1}{m_{H_2}}} \qquad (16)$$

Typical ablation cloud temperatures near the pellet are low (≅ 0.02–0.1 eV). At these temperatures hydrogen molecules have only translational and rotational energies [27]. For this reason we take $\gamma = 7/5$.

The surface temperature, $T_s$, is in turn coupled to the rate of vaporization. From kinetic theory [28] the flux of molecules leaving the pellet surface is equal to the rate at which molecules would strike the surface from its saturated vapour pressure as if the surface were in equilibrium with its vapour at temperature $T_s$. Since in equilibrium not all molecules which strike the surface recondense, the striking rate must be multiplied by a condensation coefficient, $\alpha(T_s)$, which is the fraction of molecules that are not reflected upon striking the surface of the liquid or solid.

Assuming that none of the molecules leaving the surface return and recondense, then the flux of molecules from the surface is

$$\frac{\rho_1 v_1}{m_{H_2}} = \frac{P_v(T_s)\alpha(T_s)}{\sqrt{2\pi m_{H_2} k T_s}} \qquad (17)$$

where

$$P_v(T_s) = P_o \exp \frac{-A}{T_s} + BT_s \qquad (18)$$

is the saturated vapour pressure for liquid or solid $H_2$ [13] at a temperature $T_s$. The constants $P_0$, A, and B are 4.841 X $10^7$ dynes/cm$^2$, 108.7 K and 0.0907 $K^{-1}$, respectively. The condensation coefficient $\alpha(T_s)$ is not known for hydrogen, but is taken to be unity here, as with most other insulators [29].

The energy flux and average electron energy at the pellet surface, $q_1$ and $E_1$, respectively, depend on the total integrated ablation cloud thickness from Eqs (8) and (9). It will be convenient to form the dimensionless quantities $\xi = r/r_p(t)$, and $y(\xi) = \rho(r)/\rho_1$. Using the above relations the following expressions for $q_1$ and $E_1$, at $\xi = 1$, are

$$q_1 = q_1 \frac{E_1}{E_o}$$

$$\exp - \left[ \int_{E_1}^{E_o} < \cos \theta > \hat{\sigma}_t(E')L(E')^{-1} dE' \right] \qquad (19)$$

where $q_0 = n_{e0} v_{e0}/4$. $E_0$ is the unattenuated electron energy flux, and

$$\int_{E_1}^{E_o} < \cos \theta > \frac{dE'}{L(E')} = \frac{\rho_1}{m_{H_2}} r_p(t)$$

$$X \int_1^{\infty} y(\xi) d\xi = \frac{\rho_1}{m_{H_2}} r_p(t)\Gamma \qquad (20)$$

By making use of Eqs (10) and (11) for L(E) and $\hat{\sigma}_t(E)$ respectively the integrations in Eqs (19) and (20) can be easily carried out. In Eq. (20) a "shape factor" $\Gamma = \int_1^{\infty} y(\xi) d\xi$ has been defined which indicates the magnitude of the gradient in the ablation density profile; the total integrated cloud thickness in cm$^{-2}$ is $(\rho_1/m_{H_2})r_p\Gamma$. A necessary condition for quasi-steady-state is that this quantity be finite. This is always true for spherical flows in vacuo since the velocity of such flows either increases without bound (for instance with heat addition) or approaches a limiting value, as in polytropic flows ($p = p^{\gamma}$), cf Ref. [30]. As an example, it is easy to show that an adiabatic expansion in spherical geometry has a normalized density, $y(\xi)$, given implicitly as:

$$\frac{1}{\xi^4} = y^2 \left[ \left( \frac{\gamma + 1}{\gamma - 1} \right) - \frac{2}{(\gamma - 1)} y^{\gamma - 1} \right] \qquad (21)$$

in which case $\Gamma = 0.570$ for $\gamma = 7/5$.

The expansion of the ablation cloud is not a free or adiabatic expansion. Therefore in our case the determination of the shape factor $\Gamma$ must be made in connection with the ablation cloud heating by incident electron energy deposition.

## 5. EVALUATION OF THE SHAPE FACTOR $\Gamma$

Given pellet radius $r_p(t)$, electron plasma density $n_{e0}$ and temperature $T_{e0}$, then the energy and mass balance equations (13) and (15) with the equations for the energy flux at the pellet surface (19) and (20) and the additional equations (14), (16) and (17) constitute a set of seven coupled algebraic equations with nine unknowns – $\dot{r}_p$, $T_s$, $\rho_1$, $v_1$, $T_1$, $M_1$, $q_1$, $E_1$, and the shape factor $\Gamma$. Two additional equations are needed to close the system. These are the two relations for $M_1$ and $\Gamma$ which depend upon the ablation cloud heating by the incident electrons. In this way a self-consistent solution for the pellet lifetime can be found by solving the above set of equations for $\dot{r}_p$ for a given instantaneous pellet radius $r_p$, plasma density, $n_{e0}$, and temperature, $T_{e0}$. We must now turn to the problem of the heating-up of the ablation cloud and its quasi-steady expansion. By including this important effect the dimensionless density profile, $y(\xi)$, may be obtained, which is then used to obtain the shape factor, $\Gamma$, in terms of the quantities $T_1$ and $r_p$.

Qualitatively the hydrodynamic motion of the heated flow can be described as follows: heating predominates near the surface of the pellet where absorption of the energy flux is strongest, whereas further away from the pellet radial expansion predominates over heating. It is then possible for the ablation cloud to be accelerated up to a sonic radius where heating and expansion work exactly balance and then pass over into the supersonic range where the gas is still receiving heat but it is spent mostly on the kinetic energy of the flow.

Rather than solve the equations exactly we choose to make another approximation at this point. The flow will be assumed to be sonic everywhere. This approximation then allows the remaining equations to be solved easily. The justification for this approximation is that the shape factor and the pellet lifetime are not strong functions of the velocity of the flow.

The magnetic field imposes an anisotropy on the volumetric heat source, denoted by $S_v(r)$, in the spherically expanding ablation cloud. We average the volumetric heat source term, $S_v$, over a spherical shell of volume $4\pi r^2 dr$. As pointed out earlier, the energy flux passing through a spherical surface is reduced by $f_B$ over the non-magnetic case. From Fig.1b it can easily be seen that

$$< S_v(r) > = f_B Q \frac{dq}{dr} = 1/2Q \frac{dq}{dr} \; ; \; (r_g << r_p) \tag{22}$$

where Q represents the fractional energy loss of the incident electrons which heats up the ablation cloud. As mentioned in Section 2, Q will be close to 1 for a highly collisional ablation cloud for any electron energy. Expressing Eq.(8) for q(r) in differential form and with the help of Eq.(4) results in

$$\frac{dq(r)}{dr} = n(r)q(r)\left[\frac{L(E(r))}{< \cos\theta >E(r)} + \hat{\sigma}_t(E(r))\right] \tag{23a}$$

$$= \frac{\rho(r)}{m_{H_2}} q(r)\Lambda(E(r)) \tag{23b}$$

where $\Lambda(E(r))$ in Eq.(23b) is an effective "energy flux cross-section". If G is the instantaneous ablation rate in g/s, then the mass and energy conservation equations neglecting heat conditions for the steady spherically-symmetric ablation cloud are the following:

$$\rho v r^2 = \rho_1 v_1 r_p^2 = \frac{G}{4\pi} = \text{constant} \tag{24}$$

$$\frac{1}{r^2}\frac{d}{dr}\left[r^2 \rho v \left(\frac{\gamma p}{(\gamma-1)\rho} + 1/2v^2\right)\right]$$

$$= f_B \frac{\rho}{m_{H_2}} q(r)\Lambda(r) \tag{25}$$

since $r^2 \rho v$ is constant then Eq.(25) can be expressed as

$$\frac{d}{dr}\left[\frac{\gamma p}{(\gamma-1)\rho} + 1/2v^2\right] = \frac{f_B q(r)\Lambda(r)}{m_{H_2} v(r)} \tag{26}$$

As a first approximation to the source term on the right-hand side of Eq.(26) scattering is neglected, so that $q(r) = (q_0/E_0)E(r)$, (constant particle flux), and $\Lambda(r) = L(E(r))/(\langle\cos\theta\rangle E(r))$ (note that this approximation is made only in the cloud heating equation and not in the pellet energy flux equation). Let L(E(r)) be constant and equal to $L(E_0)$. Since $\gamma p/\rho = \gamma kT/m_{H_2} = C^2$, where C is the local speed of sound, then with the above approximations Eq.(26) becomes

$$\frac{d}{dr} v(r)^2 \left(\frac{1}{2} + \frac{1}{(\gamma-1)M^2}\right) = \frac{f_B Q}{< \cos\theta >} \frac{q_o L(E_o)}{E_o m_{H_2} v(r)} \tag{27}$$

With Q(r) = 1 then solution of Eq.(27) yields

$$v(\xi) = \sqrt{\frac{\gamma kT_1}{m_{H_2}}} M(\chi(\xi-1) + 1)^{1/3} \tag{28}$$

$$T(\xi) = T_1(\chi(\xi-1) + 1)^{2/3} \tag{29}$$

$$y(\xi) = \frac{\rho(\xi)}{\rho_1} = \xi^{-2}(\chi(\xi-1) + 1)^{-1/3} \tag{30}$$

The pressure, $p(\xi)$, is then

$$p(\xi) = \frac{\rho_1 kT_1}{m_{H_2}} \xi^{-2}(\chi(\xi-1) + 1)^{1/3} \tag{31}$$

where $\chi$ is defined as

$$\chi = \frac{3}{16} \frac{m_{H_2}^{1/2}}{(\gamma kT_1)^{3/2}} \frac{n_{eo} v_{eo} L(E_o) Q r_p}{\left(\frac{M^3}{2} + \frac{M}{(\gamma-1)}\right)} \tag{32a}$$

for M = 1 this is

$$\chi = .068 \frac{n_{eo} v_{eo} L(E_o) r_p(t) Q}{(T_1)^{3/2}} \tag{32b}$$

Defining $a = (\chi-1)^{1/3}$, the expression for the shape factor, $\Gamma$, is from Eqs (20) and (30)

$$\Gamma = \begin{cases} 3/4 \text{ if } \chi = 1 \\ \frac{\chi}{(\chi-1)}\left[\left|\frac{\pi}{2a\sqrt{3}}\right| + \frac{1}{6a}\ln\left[\frac{(a+1)^2}{a^2-a+1}\right] - \frac{1}{a\sqrt{3}} \right. \\ \left. \arctan\left[\frac{2-a}{a\sqrt{3}}\right] - \frac{1}{\chi}\right] \text{ if } \chi \neq 1 \end{cases} \tag{33}$$

For the expression in Eq. (32b) the units for $L(E_0)$ are eV - $cm^2$ and $T_1$ is in Kelvin. Aside from the external plasma parameters, $\Gamma$ is a function of the instantaneous pellet radius, $r_p$, and the temperature, $T_1$, of the ablation cloud just at the pellet's surface ($\xi = 1$).

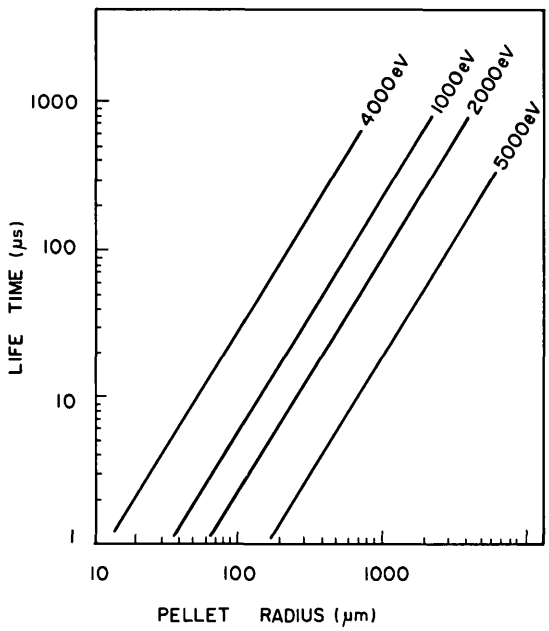


*FIG.4a. Pellet lifetime, $\tau_p$, vs initial pellet radius, $r_{p0}$, for various plasma temperatures. The plasma electron density is $4 \times 10^{13}$ $cm^{-3}$.*

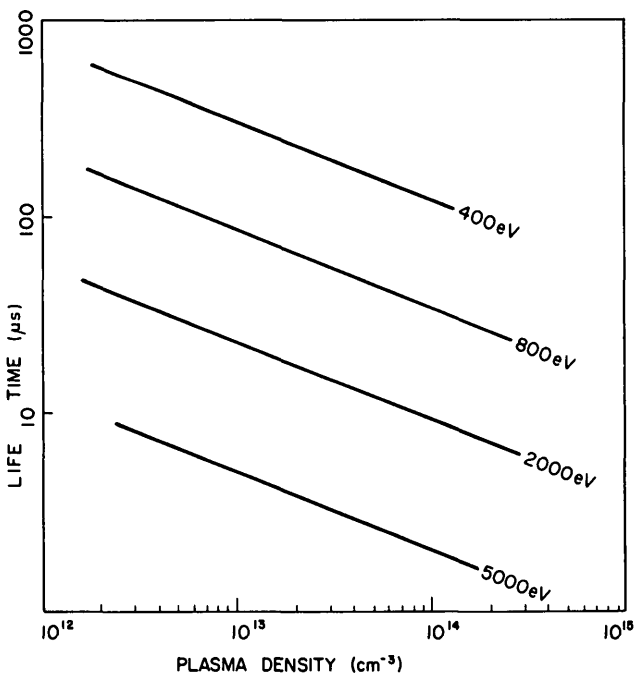


*FIG.4b. Pellet lifetime, $\tau_p$, vs plasma electron density, $n_e$, for various plasma temperatures. The pellet radius is 300 μm.*

## 6. RESULTS OF THE SONIC APPROXIMATION AND COMPARISON WITH EXPERIMENT

With the expression for $\Gamma$ as a function of $T_1$ and $\dot{r}_p$ and with M = 1, the aforementioned set of equations is now closed. $\dot{r}_p$ is found for an initial pellet radius $r_{p0}$ by solving the set of simultaneous equations numerically. By incrementing the pellet radius a new $r_p$ is found and so forth. In this way the lifetime for the pellet to decrease to 5 per cent of its original value (99.987 per cent vaporized) can be computed. The lifetimes for typical pellet radii and uniform plasma parameters are illustrated in Figs 4a and 4b.

In order to compare our model with the recent pellet injection experiment performed on the ORMAK tokamak [31], the pellets' motion through the varying plasma conditions is taken into account in the calculations of the lifetime. The experimental lifetime of 35 μm radius pellets moving 100 m/s into ORMAK was about 380 μs whereas the theoretical prediction is 381 μs. For 210 μm pellets moving at the same speed the experimental lifetime is 850 μs and the theoretical calculation gives 820 μs. Reference [31] gives a detailed description of these experiments and calculations.

## 7. SCALING LAWS AND THE IONIZATION RADIUS

From Figs 4a and 4b, one observes that the lifetime of the pellet is not a strong function of the plasma density; furthermore, the lifetime is a much stronger function of the pellet's initial radius than the obvious linear relationship. These results are not surprising in the light of certain central implications of this model. This becomes evident upon making simplifying approximations to the foregoing derivations, leading to scaling laws for the ablation cloud temperature and the pellets' lifetime in terms of $r_p$, $n_{e0}$, and $T_{e0}$.

The pellets' surface temperature, $T_s$, is a slowly varying function of the ablation rate, since only a small change in $T_s$ produces a very large change in the ablation rate [see Eqs (17) and (18)]. Further, in order for the vapour pressure relation in Eq.(18) to be meaningful the surface temperature must be below the critical point temperature for hydrogen (33 K). At this temperature the ablation rate is, from Eq.(17), $4.24 \times 10^{25}$ molecules/s/$cm^2$, which corresponds to a surface regression speed, $\dot{r}_p = 2 \times 10^3$ cm/s. However, the surface temperature does not determine the ablation rate for energy fluxes strong enough to cause

this regression speed. Instead the ablation cloud controls the ablation rate. In other words, even though we cannot apply the surface conditions above the critical temperature this model is still valid. In fact, at a surface temperature of 33K the surface conditions are almost totally insignificant because of the almost complete absorption of the electron energy flux in the ablation cloud. The following example illustrates this point clearly. An $H_2$ pellet of radius 320 $\mu$m subjected to a plasma with temperature and density 3 keV and $3.5 \times 10^{13}$ cm$^{-3}$ respectively has a lifetime of 12.33 $\mu$s; indicating a surface temperature $\sim$ 33 K. The external energy flux to the pellet is $q_0 = 1.92 \times 10^{26}$ eV/cm$^2$ per second. From Eq.(13) it is shown that the ratio of the energy flux at the pellet surface, $q_1$, to the external energy flux, $q_0$, is $q_1/q_0 \approx U_s \rho_0 \dot{r}_p/(q_0 m_{H_2}) = 0.0023$. This indicates that the ablation rate is not sensitive to the energy balance at the pellet surface, nor the details of the phase transition. Essentially what this means is that the ablation cloud controls the dynamics of pellet evaporation.

From the nature of the pellet ablation dynamics a scaling law for the ablation rate can be found. Since $T_s$ is slowly varying for a wide range of ablation rates, $T_1$ and $v_1$ may be taken to be constant in what follows. Assuming an average value for L(E), then from Eq.(20) one has

$$(E_o - E_1) = 2\, L(E_o)\, \frac{\rho_1}{m_{H_2}}\, r_p \Gamma(r_p, T_1) \qquad (34)$$

Neglecting scattering for simplicity, then from Eq.(19) and Eq.(34) the energy flux at the pellet surface is given as

$$q_1 = q_o \left[ 1 - \frac{2\rho_1}{m_{H_2}} \frac{r_p L(E_o) \Gamma(r_p, T_1)}{E_o} \right] \qquad (35)$$

Neglecting the heat capacity effect in Eq.(13), then with Eq.(35) and Eq.(15) the surface regression speed is

$$\dot{r}_p = \left( \frac{1}{\rho_o / m_{H_2}} \right) \left\{ \frac{q_o}{\frac{U_s}{f_H f_B} + \frac{2 q_o r_p \Gamma(r_p, T_1) L(E_o)}{v_1 E_o}} \right\} \qquad (36)$$

Here again, the insensitivity of the boundary conditions at the pellet surface is apparent. The first term on the left-hand side of the denominator in the above equation contains the sublimation energy $U_s$. This term can be neglected in comparison with the term on its right provided that:

$$\frac{v_1 E_o U_s}{2 f_H f_B q_o r_p \Gamma L(E_o)} = \frac{2 v_1 U_s}{f_H f_B n_{eo} v_{eo} r_p \Gamma L(E_o)} \equiv \epsilon_h << 1 \qquad (37)$$

For instance, in keeping with the above example where $T_{eo} = 3$ keV, $n_{eo} = 3.5 \times 10^{13}$ cm$^{-3}$, $r_p = 320\ \mu$m; $L(E_0) = 2.91 \times 10^{-16}$ eV/cm$^2$, $\Gamma(r_p, T_1) = 0.20$, $v_1 = 4 \times 10^4$ cm/s, $\epsilon_h = 0.0137$. The implication is as follows: when $\epsilon_h$ is large, e.g. with low plasma density or small pellet radius, the ablation rate is primarily controlled by the conditions at the pellet surface, since the ablation cloud is very "thin". Increasing the energy flux, in particular the electron density, increases the surface regression rate. Thus the total ablation cloud thickness increases up to a point where it is limited by the electron range, which is strongly dependent on the plasma temperature. At this point $\epsilon_h$ is very small, so that the role of the ablation cloud dominates the ablation rate. $U_s$ is negligible, as if $U_s \to 0$. This also implies that the electron energy flux at the pellet surface, $q_1$, is negligible since

$$\frac{4\pi r_p^2 q_1}{\frac{U_s}{m_{H_2}}} = \lim_{\substack{U_s \to 0 \\ q_1 \to 0}} G = 4\pi \rho_o r_p^2 \dot{r}_p : \quad G \text{ is finite} \qquad (38)$$

Provided Eq.(37) is fulfilled, Eq.(36) also predicts that increases in plasma density even further have little effect on the ablation rate. Physically, this is because a denser ablation cloud would result if the ablation rate were increased. This cannot be so since the electrons would not even reach the pellet surface; they are already "range-limited". The effect of the plasma density is important in the sonic approximation insofar as the heating of the vapour and hence the shape factor $\Gamma$ is affected, i.e. increased heating reduces the shape factor $\Gamma$ or "tapers" the ablation cloud more because the flow velocity increases. Thus, in order to maintain the "range-limited" thickness the pellet ablates at a slightly faster rate upon increase of plasma density in order to compensate.

Increases in the pellet radius cause the total integrated thickness of the ablation cloud to increase proportionally because the distance required in order for the ablation cloud density to fall to any given value is increased.

Therefore, to maintain "range-limited" conditions, the gas density at the pellet surface, $\rho_1$, hence the surface regression speed, must decrease accordingly, giving rise to the $\sim r_p^{-1}$ dependence of $\dot{r}_p$ in Eq.(36). The "range-limited" concept is similar in principle to Krokhin's [32] self-matched regime where the optical thickness of materials heated by intense laser light tends to remain at a constant value throughout the course of heating. In our case, though, the pellets' radius, in a manner of speaking, determines the "optical thickness".

The value of $\chi$, given by Eq.(32), is in practically all cases of interest much larger than unity; and the dominant term in Eq.(33) is the first term on the right-hand side in the brackets. Thus, $\Gamma \sim \chi^{-1/3} \sim v_1\, m_{H_2}^{-1/6}\, Q^{-1/3}\, n_{eo}^{-1/3}\, L(E_0)^{-1/3}\, T_{eo}^{-1/6}$, which when substituted into Eq.(36) gives the following scaling laws for $\dot{r}_p$, pellet lifetime; $\tau_p$, and ablation cloud temperature one pellet radius away from the surface, $T_{(\xi=2)}$.

$$\dot{r}_p = 6.29 \times 10^5 \frac{Q^{1/3} n_{eo}^{1/3} T_{eo}^{7/6}}{r_p^{2/3}} \times \left[\frac{1}{L(E_o)}\right]^{2/3} \frac{1}{n_o M_o^{1/3}} \quad \text{cm/s} \qquad (39)$$

$$\tau_p = \frac{\int_o^{r_{po}} r_p^{2/3} dr_p}{r_{po}^{2/3} \dot{r}_p (r=r_{po})}$$

$$= .867 \frac{r_{po}^{5/3} L(E_o)^{2/3} n_o M_o^{1/3}}{Q^{1/3} n_{eo}^{1/3} T_{eo}^{7/6}} \quad \mu s \qquad (40)$$

$$T_{(\xi=2)} = 1.88 (r_p n_{eo} Q)^{2/3} T_{eo}^{1/3} L(E_o)^{2/3} M_o^{1/3} \text{ eV} \qquad (41)$$

Here $n_0 = \rho_0/m_{H_2}$ is the solid molecular number density, $T_{eo}$ is in eV, $r_p$ in cm, and $M_0$ is the molecular mass of the pellet in atomic mass units. $D_2$ and $T_2$ pellets have slightly higher number densities and molecular masses, providing a small but noticeable increase in lifetimes over $H_2$ pellets. Note, also the strong dependence of $\tau_p$ on the pellet radius and the weak dependence on the plasma density in accordance with the above description of the ablation dynamics. We point out further that the scaling laws are independent of the velocity of the ablation cloud at the pellet surface, $v_1$. This reinforces our conclusions that the surface conditions play an insignificant role in the ablation dynamics for small $\epsilon_h$.

The small inverse effect the plasma temperature has on the ablation cloud temperature $T_a$ can be shown by expressing L(E) in the limit of high energy, i.e. $L(E) \propto 1/E^{0.832}$. Therefore, $T_a \propto T_{eo}^{-0.215}$. This inverse effect is due to the fact that the *production* of vapour outweighs the additional heating: a slightly cooler ablation cloud results.

By approximating the local Mach number in the flow, M(r), by a constant M = 1 we have underestimated the ablation cloud temperature near the pellet (where we expect subsonic flow) by a factor of $\sim M(r)^{2/3}$ [see Eqs (29) and (32)].

For example, if $n_{eo} = 4 \times 10^{13}$ cm$^{-3}$, $T_{eo} = 5000$ eV, $r_p = 0.03$ cm, then from Eq.(41) $T_{(\xi=2)} = 0.152$ eV. If we take $M_{(\xi=2)} = 1/2$ then $T_{(\xi=2)} = 0.240$ eV. One should expect the actual temperature near the pellet to be higher than that in the sonic approximation because according to Eq.(28) the flow velocity $\sim M(r)^{2/3}$. This means that the flow actually expands more slowly and hence spends more time heating up. However the ablation rate as given by the sonic approximation should not differ too much from reality. This is because the flow velocity has likewise been underestimated in the supersonic portion of the ablation cloud. Therefore the sonic approximation overestimates the thickness of the ablation cloud in this region.

At this point we can establish reasonable grounds for the credibility of the quasi-steady approximation. In order for quasi-steady conditions to prevail, the fractional change in pellet radius must be small in the time for the ablation cloud to be fully developed (at least over a pellet radius). If this is true then the expression for $\tau_p$ given by Eq.(40) is valid. Let us define a characteristic time for the ablation cloud to be fully developed as $\tau_{ablation}$, where

$$\tau_{ablation} = \frac{r_p}{V_{(\xi=2)}} = \frac{r_p}{\sqrt{\frac{\gamma k T_{(\xi=2)}}{m_{H_2}}}} \qquad (42)$$

In this amount of time the pellet's radius changes by $\delta r_p$ where

$$\frac{\delta r_p}{r_p} = \frac{\dot{r}_p \tau_{ablation}}{r_p} = \frac{\dot{r}_p}{\sqrt{\frac{\gamma k T_{(\xi=2)}}{m_{H_2}}}} \qquad (43)$$

Using the scaling laws Eq. (39) and Eq. (41) in the above expression we find

$$\frac{\delta r_p}{r_p} \sim \frac{E_o}{n_o L(E_o) r_p} \sim \theta \frac{Re}{r_p} \qquad (44)$$

Where Re is the range of an incident unattenuated plasma electron in the solid pellet of molecular number density $n_0$. It is not surprising that $\delta r_p/r_p$ should depend only on the range of the incident electron in the solid. This is because more material is needed to shield the pellet from electrons with larger ranges. If the range becomes too large, a point is reached where there is not enough material in the pellet to produce a fully developed ablation cloud. Pushed to the extreme, one can imagine ranges so large that volumetric heating of the pellet takes place, in which case the time scales for pellet disassembly and gas-dynamic expansion are the same. For most plausible combinations of pellet radii and plasma temperatures, $\delta r_p/r_p$ is indeed quite small. On the basis of these results, it is concluded that the quasi-steady model is reasonably good. Thus, the pellet lifetime, $\tau_p$, given by Eq.(40) is meaningful. The neglect of heat conduction in the ablation cloud can be justified on the basis of the scaling laws. For $H_2$ gas the thermal diffusivity in cgs units is $\alpha = 3 \times 10^{19} T^{1/2} n^{-1}$ [28] where T is in eV and n is the number density ($cm^{-3}$). The characteristic velocity of heat transport in the ablation cloud in a characteristic distance $\delta$ is $v_H \sim (\alpha v/\delta)^{1/2}$ where v is the flow velocity. Thus $v_H/v \sim 6.4 \times 10^6 (1/M n\delta)^{1/2}$ where M is the local Mach number of the flow. For all cases of interest $v_H/v \ll 1$ so that heat conduction is ignorable. In fact this is true even near the pellet, where M and $\delta$ decrease and n increases quite rapidly [see Eq. (30)].

Finally, an a posteriori justification for the large fraction of neutral molecules in the ablation cloud can be given at this point. The "ionization radius" $r_I$, defined in Eq.(1), can be obtained by first assuming that $\tau_{ei}$ is constant everywhere in the ablation cloud and that

$$\tau_{ei} = \left( \frac{n_{e0} \sigma_{ei}(E_0) \bar{v}_{e0}}{4} \right)^{-1}$$

Here $\sigma_{ei}(E)$ is the cross-section for ionization of $H_2$ by electron impact [20]. Substituting the flow velocity $v(\xi)$ from Eq.(28) into Eq.(1) yields after integration

$$\xi_I = \frac{r_I}{r_p} = \frac{1}{\chi} \left[ \frac{2\chi v_1 \tau_{ei} + 1}{3 r_p} \right]^{3/2} + \frac{\chi - 1}{\chi} \qquad (45)$$

For typical parameters and pellet sizes in the domain where our model is valid, $\xi_I$ is given in Table I. It is interesting to point out that at the ionization radius the temperature of the ablation cloud using Eq.(29) and Eq.(45) is given by $T_I \sim 0.037 \langle L(E_0) \rangle / \sigma_{ei}(E_0) \cong 2.5$ eV independent of $r_p$, $n_{e0}$ and $T_{e0}$. This result is close to the temperature 2.02 eV that Gralnick [4]

TABLE I. IONIZATION RADIUS NORMALIZED TO PELLET RADIUS FOR NEUTRAL ABLATION CLOUD AS A FUNCTION OF PLASMA TEMPERATURE AND DENSITY

($\xi_I = r_I/r_p$)

| $T_{e0}$ (ev.) | $\xi_I$ | | | | | |
|---|---|---|---|---|---|---|
| | $n_{e0} = 10^{13}$ cm$^{-3}$ | | $n_{e0} = 5 \times 10^{13}$ | | $n_{e0} = 1 \times 10^{14}$ | |
| | $r_p = 0.02$ | $r_p = 0.05$ | $r_p = 0.05$ | $r_p = 0.1$ | $r_p = 0.1$ | $r_p = 0.2$ |
| 200 | 333 | 134 | 27.4 | 14.2 | 7.57 | 4.28 |
| 500 | 414 | 166 | 34 | 17.5 | 9.1 | 5.05 |
| 1000 | 635 | 255 | 51.7 | 26.4 | 13.7 | 7.35 |
| 5000 | 1282 | 513 | 103 | 52 | 26.6 | 13.8 |

obtained for the ablatant just at the pellet surface where in his analysis complete ionization of the surface takes place.

At this point one can discover whether or not the ionized portion of the ablation cloud has enough pressure to create a $\beta = 1$, or "magnetic bubble", under CTR conditions, as Rose [2] predicts. A reasonable criterion for this to occur would be that the pressure in that ablation cloud at the ionization radius, $P_I$, be greater than or equal to the embedded magnetic field pressure $B^2/8\pi$ in the plasma. The ablation cloud pressure at the ionization radius, $P_I$, can be found by eliminating $\rho_1$ in Eq.(31) with the help of Eq.(15) and Eq.(39), viz.,

$$p_I = \frac{9.6 \times 10^{-8} L(E_0)^{4/3} T_{e0}^{13/6} n_{e0}^{7/3} r_{p0}^{4/3}}{Q^{2/3}} \text{ dynes/cm}^2 \tag{46}$$

For typical plasma parameters characteristic of EPR designs [34], $T_{e0} = 1.5 \times 10^4$ eV, $n_{e0} = 1.8 \times 10^{14}$ cm$^{-3}$, and B = 37 kG. For an $H_2$ pellet with $r_{p0} = 0.3$ cm, ($\tau_p = 25$ $\mu$s), $\xi_I = 8.5$, and $p_I/(B^2/8\pi) = 0.16$. This means that a magnetic bubble as postulated by Rose will probably not form, as also suggested by Chang [3]. The plasma in the ablation cloud at the ionization radius is still highly collisional, in fact $\omega_{ci}\nu_{ii}$ is much less than 1 but will increase further away from the pellet as the temperature in the ablation cloud is continually increasing and the density decreasing. This leads us to believe that a spherical expansion prevails at least in the vicinity of the pellet where almost total absorption of the incident electron energy flux takes place.

## 8. CONCLUSION

From the foregoing analysis as a whole it follows that the most important role in the solid hydrogen-plasma interaction is that nearly total shielding of the pellet by its own neutral ablatant occurs through the establishment of a dense ablation cloud. The integrated cloud density is largely determined by the pellet size and governs the ablation rate by maintaining a "range-limited" cloud thickness. Above plasma densities of $10^{13}$ cm$^{-3}$ the exact details of the boundary conditions at the pellet surface become immaterial except possibly in determining $T_1$, which is used in the determination of $\Gamma$.

Because of the large ionization radius compared to the pellet size and the very low temperature of the ablatant ($\leqslant 0.1$ eV) if $T_e < 5$ keV, $n_e < 5 \times 10^{13}$ cm$^{-3}$, we do not expect the magnetic field to alter the "spherical" expansion near the pellet where shielding is most effective.

The model gives a good agreement with the recent pellet injection experiment performed on the ORMAK tokamak. It is to be hoped other experiments will be performed using larger pellets and faster injection speeds so that the scaling laws for the pellet lifetime and surface regression speed can be tested over a wide range of plasma densities and temperatures.

## APPENDIX

## DERIVATION OF $\sigma_B(\theta,E)$ AND $\sigma_{MS}(E)$

In this appendix the backscattering cross section, $\sigma_B(\theta,E)$, introduced below Eq. (4) is determined. A polar coordinate system (see Fig. 2) is imposed such that the z-axis is orientated along the magnetic field and points in the direction of the pellet. The velocity vector, $\vec{V}$, of the electron before the collision lies in the xz plane and has a pitch angle $\theta$ (after collision its velocity is $\vec{V}'$ and it has a new pitch angle $\theta'$) and scatters through an angle $\xi$ with respect to $\vec{V}$. $|\vec{V}| \simeq |\vec{V}'|$. The solid angle into

which the electron is scattered is sin θ' dθ' dφ'; therefore a differential scattering cross-section for scattering from θ to θ', 0 to φ' is

$$\frac{d\phi(\xi)}{d\Omega} \sin\theta' \, d\theta' \, d\phi' \tag{A1}$$

whence it follows that an effective differential scattering cross-section for scattering from θ to θ' anywhere in the annular strip 2π sin θ' dθ' becomes

$$P(\theta,\theta') \sin\theta' \, d\theta' = \int_0^{2\pi} \frac{d\sigma(\xi)}{d\Omega} \sin\theta' \, d\theta' \, d\phi' \tag{A2}$$

Equation (A2) is now a "pitch angle" differential scattering cross-section. To evaluate Eq. (A2), the Euler relation is invoked, viz.,

$$\cos\xi = \cos\theta \cos\theta' + \sin\theta \sin\theta' \cos\phi' \tag{A3}$$

The expression for the differential elastic scattering cross-section for electrons on hydrogen [18] is given by

$$\frac{d\sigma(\xi)}{d\Omega} = \frac{\sigma_o[2 + 2\varepsilon(1 - \cos\xi)]^2}{[1 + 2\varepsilon(1 - \cos\xi)]^4} \tag{A4}$$

where $\sigma_o = \dfrac{4\pi^4 m_e^2 e^4 a_o^4}{h^4}$; the dimensionless energy of the electron, $\varepsilon = E \Big/ \left(\dfrac{2\hbar^2}{m_e a_o^2}\right)$; and $a_o$ and E are the Bohr radius and electron energies in ergs, respectively. Substituting Eq. (A3) into Eq. (A4) and Eq. (A4) into Eq. (A2), one has, after some rearrangement,

$$P(0,\theta') \sin\theta' \, d\theta' = \sigma_o \sin\theta' \, d\theta' \int_0^{2\pi} \frac{A^2 + 2AB\cos\phi + B^2\cos^2\phi}{[C + B\cos\phi]^4} \, d\phi \tag{A5}$$

where

$$A = 2 + 2\varepsilon - 2\varepsilon\cos\theta\cos\theta'$$

$$B = 2\sin\theta\sin\theta'$$

$$C = A - 1 \, . \tag{A6}$$

Since $C^2 > B^2$, then $\int_0^{2\pi} \rightarrow 2\int_0^{\pi}$, and Eq. (A5) can be integrated to obtain

$$P(\theta,\theta')\sin\theta'\,d\theta' = \frac{\sigma_o \pi}{(C^2 - B^2)^{7/2}} \times \{2A^2C^3 - 8AB^2C^2 + 3A^2B^2C - 2AB^4 + B^2C^3 + 4B^4C\} \times \sin\theta'\,d\theta' \qquad (A7)$$

Inspection of Eq. (A7) shows that as $\theta \rightarrow 0$, $P(0,\theta') \rightarrow 2\pi\sigma_o \frac{d\sigma(\theta')}{d\Omega}$ because $\xi \rightarrow \theta'$.

The backscattering cross-section for electrons with initial pitch angle $\theta$ and dimensionless energy $\varepsilon$ is given by

$$\sigma_B(\theta,\varepsilon) = \int_{\pi/2}^{\pi} p(\theta,\theta')\sin\theta'\,d\theta' = \int_{-1}^{0} P(\mu,\mu')\,d\mu' \qquad (A8)$$

So,

$$\frac{\sigma_B(\theta,\varepsilon)}{\sigma_o\pi} = A_o I + \left[\frac{1}{5c}\left(\frac{1}{\Delta} - \frac{1}{a^{5/2}}\right) - \frac{b}{2c} I\right] A_1 + \left[\frac{-1}{4\Delta c}\left(1 + \frac{3b}{10c}\right) + \frac{3b}{40c^2a^{5/2}} + \frac{1}{c}\left(\frac{a}{4} + \frac{3b^2}{16c}\right) I\right] A_2 + \left[\frac{1}{\Delta c}\left(\frac{1}{3} + \frac{2a}{15c} + \frac{b}{24c} + \frac{b^2}{80c^2}\right) - \frac{1}{a^{5/2}c^2}\left(\frac{2a}{15} + \frac{b^2}{80c}\right) - \frac{1}{c^2}\left(\frac{3ab}{8} + \frac{b^3}{32c}\right) I\right] A_3 + \left[\frac{1}{\Delta c}\left(\frac{-1}{2} - \frac{3a}{8c} + \frac{b}{12c} - \frac{19ab}{240c^2} + \frac{b^2}{96c^2} + \frac{b^3}{320c^3}\right) + \frac{1}{a^{5/2}c^3}\left(\frac{19ab}{240} - \frac{b^3}{320c}\right) + \frac{1}{c^2}\left(\frac{3a^2}{8} + \frac{3ab^2}{16c} - \frac{b^4}{128c^2}\right) I\right] A_4 + \left[\frac{1}{\Delta c}\left(1 + \frac{4a}{3c} - \frac{3b}{4c} + \frac{8a^2}{15c^2} - \frac{19ab}{48c^2} + \frac{b^2}{8c^2} - \frac{11ab^2}{160c^3} + \frac{b^3}{64c^3} + \frac{3b^4}{640c^4}\right) - \frac{1}{a^{5/2}c^3}\left(\frac{8a^2}{15} + \frac{3b^4}{640c^2}\right) + \frac{1}{c^3}\left(\frac{-15a^2b}{16} + \frac{5}{32}\frac{ab^3}{c} - \frac{3b^5}{256c^2}\right) I\right] A_5 \qquad (A9)$$

where

$$a = 1 + 4\varepsilon + 4\varepsilon^2\mu^2,\quad c = 4\varepsilon^2$$

$$\Delta = (a - b + c)^{5/2}$$

$$b = -(4\varepsilon\mu + 8\varepsilon^2\mu),\quad \mu = \cos\theta,\quad \ell = 2(1 + \varepsilon),\quad \beta = 2\varepsilon\mu$$

$$A_o = 2\ell^5-6\ell^4+6\ell^3-2\ell^2+4\varepsilon^2(1-\mu^2)[-4\ell^3+10\ell^2-5\ell-1] + 64\varepsilon^5(1-\mu^2)^2$$

$$A_1 = -10\ell^4\beta+24\ell^3\beta-18\ell^2\beta+4\ell\beta+4\beta\varepsilon^2(1-\mu^2)[12\ell^2-10\ell+5] - 64\varepsilon^5\mu(1-\mu^2)^2$$

$$A_2 = 20\ell^3\beta^2-36\ell^2\beta^2+18\ell\beta^2-2\beta^2+4\varepsilon^2(1-\mu^2)[-12\ell\beta^2+10\beta^2+4\ell^3-10\ell^2+5\ell+1] - 128\varepsilon^5(1-\mu^2)^2$$

$$A_3 = -20\ell^2\beta^3+24\ell\beta^3-6\beta^3+4\varepsilon^2\beta(1-\mu^2)[4\beta^2-12\ell^2+10\ell-5] + 128\varepsilon^5\mu(1-\mu^2)^2$$

$$A_4 = 2\beta^4(5\ell-3)+ 8\varepsilon^2\beta^2(1-\mu^2)[6\ell-5] + 64\varepsilon^5(1-\mu^2)^2$$

$$A_5 = -2\beta^5-16\beta^3\varepsilon^2(1-\mu^2) - 64\varepsilon^5\mu(1-\mu^2)^2$$

and

$$I = \frac{2b}{5(4ac - b^2)a^{5/2}}\left\{1 + \frac{16ac}{3(4ac - b^2)} + \frac{128a^2c^2}{3(4ac - b^2)^2}\right\}$$

$$+ \frac{2(2c - b)}{5(4ac - b^2)(a - b + c)^{5/2}}\left\{1 + \frac{16c(a - b + c)}{3(4ac - b^2)} + \frac{128c^2(a - b + c)^2}{3(4ac - b^2)^2}\right\}$$

It is reassuring to note that $\sigma_B(\theta = \frac{\pi}{2}, \varepsilon)$ is one half of the total cross-section as it should be, i.e.,

$$\sigma_B(\theta = \pi/2, \varepsilon) = 8\pi\sigma_o \frac{3 + 18\varepsilon + 28\varepsilon^2}{3(1 + 4\varepsilon^2)^3} \tag{A10}$$

The multiple scattering cross-section $\sigma_{MS}$ can be obtained by considering the cumulative small angle scattering events which lead to a total mean square deflection angle $< \xi^2 >$ in a distance z:

$$<\xi^2> = 2\pi nz \int_0^{\pi/2} \frac{\xi^2\, d\sigma(\xi)}{d\Omega} \sin\xi\, d\xi \tag{A11}$$

From (A10) the cross-section for 90° scattering by multiple collisions, $\sigma_{MS}(E)$, is usually defined as (setting $< \xi^2 > = 1$ [35]

$$\sigma_{MS}(E) = 2\pi \int_0^{\pi/2} \xi^2 \frac{d\sigma}{d\Omega} \sin\xi\, d\xi \tag{A12}$$

which, after substituting (A4) into (A11), becomes

$$\sigma_{MS}(E) = \frac{4\pi^5 m^2 e^4 a^4 o 1}{\mu^4 \varepsilon^2}\left[\frac{(1 + \varepsilon)^3 \ln(1 + \varepsilon) - \varepsilon - \varepsilon^2/2}{(1 + \varepsilon^3)}\right] \tag{A13}$$

## REFERENCES


[1] SPITZER, Jr., L., GROVE, D.J., JOHNSON, W.E., TONKS, L., WESTENDORP, W.R., Problems of the Stellarator as a Useful Power Source, USAEC Report NYO 6047 (1954).

[2] ROSE, D.J., Culham Laboratory Technology Division, Memorandum No. 82 (1968).

[3] CHANG, C.T., Nucl. Fusion **15** (1975) 595.

[4] GRALNICK, S.L., Nucl. Fusion **13** (1973) 703.

[5] GRALNICK, S.L., A Fusion Power Plant (MILLS, R.G., Ed.), Princeton Plasma Physics Laboratory Rep, MATT–1050 (1974), Chapter 7.

[6] PETERSON, L.R., GREEN, A.E.S., J. Phys., B. (London) Ser. 2, **1** (1968) 1131.

[7] MILES, W.T., THOMPSON, R., GREEN, A.E.S., J. Appl. Phys. **43** (1972) 678.

[8] PEART, B., DOLDER, K.T., J. Phys., B. (London) **7** (1974) 236.

[9] McGOWAN, J.W., CAUDANO, R., KEYSER, J., Phys. Rev. Lett. **36** (1976) 1447.

[10] DUNN, G.H., VAN ZYL, B., Phys. Rev. **154** (1967) 40.

[11] CHRISTOFFERSEN, R.E., Configuration-interaction study of the ground state of the $H_3^+$ molecule, J. Chem. Phys. **41** (1964) 960.

[12] FURTH, H.P., Nucl. Fusion **15** (1975) 487.

[13] JOHNSON, V.J., Properties of Materials at Low Temperature (Phase 1), Pergamon Press (1961).

[14] SORENSEN, H., Nucl. Instrum. Methods **132** (1976) 377.

[15] GOUDSMIT, S., SAUNDERSON, J.L., Phys. Rev. **57** (1940) 24 and **58** (1940) 36.

[16] LEWIS, H.W., Phys. Rev. **78** (1950) 526.

[17] SPENCER, L.V., Phys. Rev. **98** (1955) 1597.

[18] MOTT, N.F., MASSEY, H.S.W., The Theory of Atomic Collisions, Oxford University Press (1965) 455.

[19] MAECKER, H.T., SCHENK, H., PETERS, W.J., Z. Phys. **140** (1955) 119.

[20] MILES, W.T., THOMPSON, R., GREEN, A.E.S., J. Appl. Phys. **43** (1972) 678; also private communication (1975).

[21] ANDERSEN, R., Atomic Data **3** (1971) 227.

[22] GELLER, R., Report EUR. CEA. FC 647 (1972).

[23] PARKS, P.B., Model of an Ablating Solid Hydrogen Pellet in a Plasma, Ph.D. Thesis, University of Illinois, Urbana (1977).

[24] RODER, H.M., CHILD, G.E., McCARTY, R.D., ANGERHOFER, P.E., NBS Technical Note 641, National Bureau of Standards, Boulder, Colorado (1973).

[25] ALLEN, H.J., "On the motion and ablation of meteoric bodies", in Aeronautics and Astronautics (HOFF, N.J., VINCENTI, W.G., Eds) Pergamon Press, New York (1960) 378.

[26] OPIK, E.J., Physics of Meteor Flight in the Atmosphere, Interscience, New York (1958) Chapter 4.

[27] OWCZAREK, J.A., Fundamentals of Gas Dynamics, International Textbook Co., Scranton, Pennsylvania (1964) 115.

[28] REIF, F., Fundamentals of Statistical and Thermal Physics, McGraw-Hill, New York (1965) 271.

[29] MAA, J.R., Ind. Eng. Chem. Fundam. **6** (1967) 504.

[30] SHAPIRO, A.H., The Dynamics and Thermodynamics of Compressible Fluid Flow, The Ronald Press Company, New York (1973).

[31] FOSTER, C.A., KIM, K., COLCHIN, R.J., MILORA, S.L., TURNBULL, R.J., Solid hydrogen pellet injection into the ORMAK tokamak (to be published).

[32] KROKHIN, O.N., Sov. Phys.-Tech. Phys. **9** (1965) 1024.

[33] RAPP, D., ENGLANDER-GOLDEN, P., J. Chem. Phys. **43** (1965) 1464.

[34] DAVIS, J.W., KULCINSKI, G.L., Nucl. Fusion **16** (1976) 335.

[35] KRALL, N.A., TRIVELPIECE, A.W., Principles of Plasma Physics, McGraw-Hill, New York (1973) 293.


(Manuscript received 13 July 1976
Final version received 28 January 1977)